https://doi.org/10.5194/wes-2025-18
Preprint. Discussion started: 10 March 2025
© Author(s) 2025. CC BY 4.0 License.

eawe european academy of wind energy
Open Access WIND ENERGY SCIENCE DISCUSSIONS

PLL-Reinforced Damping for Interoperability Enhancement of Independently Designed Grid-Forming Wind Turbines in Weak Grids

Sulav Ghimire[1,2], Gabriele Amico[3], Kanakesh VattaKkuni[1], Kim H. Jensen[1], and Guangya Yang[2]

[1]Siemens Gamesa Renewable Energy A/S, 2800 Kgs Lyngby, Denmark
[2]Technical University of Denmark, 2800 Kgs Lyngby, Denmark
[3]Siemens Gamesa Renewable Energy, G28LR Glasgow, United Kingdom

Correspondence: Sulav Ghimire (sulav.ghimire@siemensgamesa.com)

Abstract. Interoperability of grid-forming (GFM) converters is crucial for the stability and efficiency of modern power systems, particularly when two independently designed GFM converters with different control architectures are connected to a common weak AC network. In this context, the interoperability of such GFM-based generation sources is examined in this paper in terms of power and frequency oscillations during both steady-state and transient cases. Based on this analysis, a novel method of oscillation mitigation via frequency-power reference ($\omega - P^*$) droop-based feedback control in the power control loops is proposed. This method significantly improves the interoperability of grid-connected GFM converters during both steady-state and fault conditions. Furthermore, due to the generality of the control structures, the proposed method benefits different applications irrespective of the generation sources, such as offshore wind power plants (OF WPPs), GFM-HVDC converters, and battery energy storage systems (BESS). Additionally, the proposed method could reinforce standard power controller designs, such as virtual synchronous machines (VSM) or PI-controller-based power control loops.

1 Introduction

Upcoming deployment of grid-forming (GFM) converter integrated generation sources in the power grid leads to a situation where multiple inverter-based resources (IBRs) have to operate in close electrical proximity. Such IBRs developed by different original equipment manufacturers (OEMs) and developers can have different control structures. IBRs with different control structures, different control tunings, and operating in close electrical proximity can lead to control interactions resulting in power and frequency oscillation between the generation sources (Ghimire et al., 2024). Careful control tuning is necessary to avoid such interactions; however, in a multi-converter system with independently designed GFM converters – as suggested by (Ghimire et al., 2024) – the voltage-source nature of GFM converters can additionally demand control structure redesign to improve interoperability. Further, in a multi-converter system with GFM converters supplied by different vendors, one device's control structure and tuning parameters are unavailable to the other parties due to intellectual property concerns. This means that for interoperability enhancement, two general paths can be followed. The first option is to develop and build elaborate multi-party cooperation such as (InterOPERA Consortium, 2023) to perform studies and update converter control parameter

https://doi.org/10.5194/wes-2025-18
Preprint. Discussion started: 10 March 2025
© Author(s) 2025. CC BY 4.0 License.

eawe european academy of wind energy
Open Access WIND ENERGY SCIENCE DISCUSSIONS

tuning. The second option is to propose a solution of a general nature – such as the one proposed in this paper – to improve the system interoperability irrespective of the individual converters' control structure and tuning.

Only a minimal number of research works have been conducted on this subject as the topic itself falls under a growing research area with numerous changes. Further, the research works available in the academic literature rarely focus on multi-converter systems but instead on intra-generation system oscillations and interaction studies. For example, a small-signal stability study of oscillations and control interactions of GFM converters in a multi-machine setup (IEEE 39 bus system) was presented in (Benedetti et al., 2022), where the authors attributed the multi-unit interactions to the inner voltage control damping factor and the electromechanical interactions to the inner current control loop. Similarly, another study focused on the interaction between GFM converters and synchronous machines (Tayyebi et al., 2019); however, the interacting devices in the presented study were not connected in high electrical proximity. Previous works have addressed the issues of power oscillations in an inverter-based system during contingencies and provide a solution to such problems via a power oscillation damping (POD) method, which achieves the same result as a power system stabilizer (PSS) in a conventional power system (Maleki et al., 2022) - although a critical study, it does not address the oscillation issues of a multi-converter system. Academic literature also includes research on POD via GFM converters; for example, a washout filter and lead-lag compensator of appropriate control parameter design is used in the active and reactive power loops (Piepka et al., 2024). Although the washout filter helps with POD, it does not allow the slow frequency-active power droop needed for interoperability.

Recent work on the interoperability of independently designed GFM converters showed that GFM converters connected to the same PCC and operating near their operational limits exhibit 2-20 Hz oscillations around their voltage controller dead-bands (Denninger et al., 2024). The analysis highlights the risk of operating GFM converters in electrically proximal locations. The authors showed that such GFM converters undergo significant reactive power exchange, leading to irrecoverable system states. The issue of control oscillation between electrically proximal GFM converters was also studied and elaborated by the authors in their previous work (Ghimire et al., 2024). To mitigate the oscillation issues, the previous work suggested power system network design approaches and control architecture changes; however, no exact control architecture changes were suggested. This paper provides an oscillation mitigation strategy via the GFM control architecture change. To that regard, this paper is an extension or a continuation of the author's previous work (Ghimire et al., 2024).

The paper structure is as follows: Section 2 presents the test system description and an overview of the mathematical models of the GFM controls used in this paper. Section 3 presents the proposed solution method of additional frequency-active power damping to minimize the oscillations in a multi-converter system, and Section 4 presents the system response to grid events after the solution method has been applied. Considering the studies and test results presented in Section 4, Section 5 updates the solution method for a robust operation over a broader range of grid events. Finally, Section 6 concludes the paper.

2 System Description and Modeling

A network with two generation sources with different GFM control architectures is connected to the grid with a nominal SCR value of 1.6 and $X_g/R_g = 5$ as shown in Fig. 1 is considered for this paper. This SCR value qualifies our test system as a

https://doi.org/10.5194/wes-2025-18
Preprint. Discussion started: 10 March 2025
© Author(s) 2025. CC BY 4.0 License.

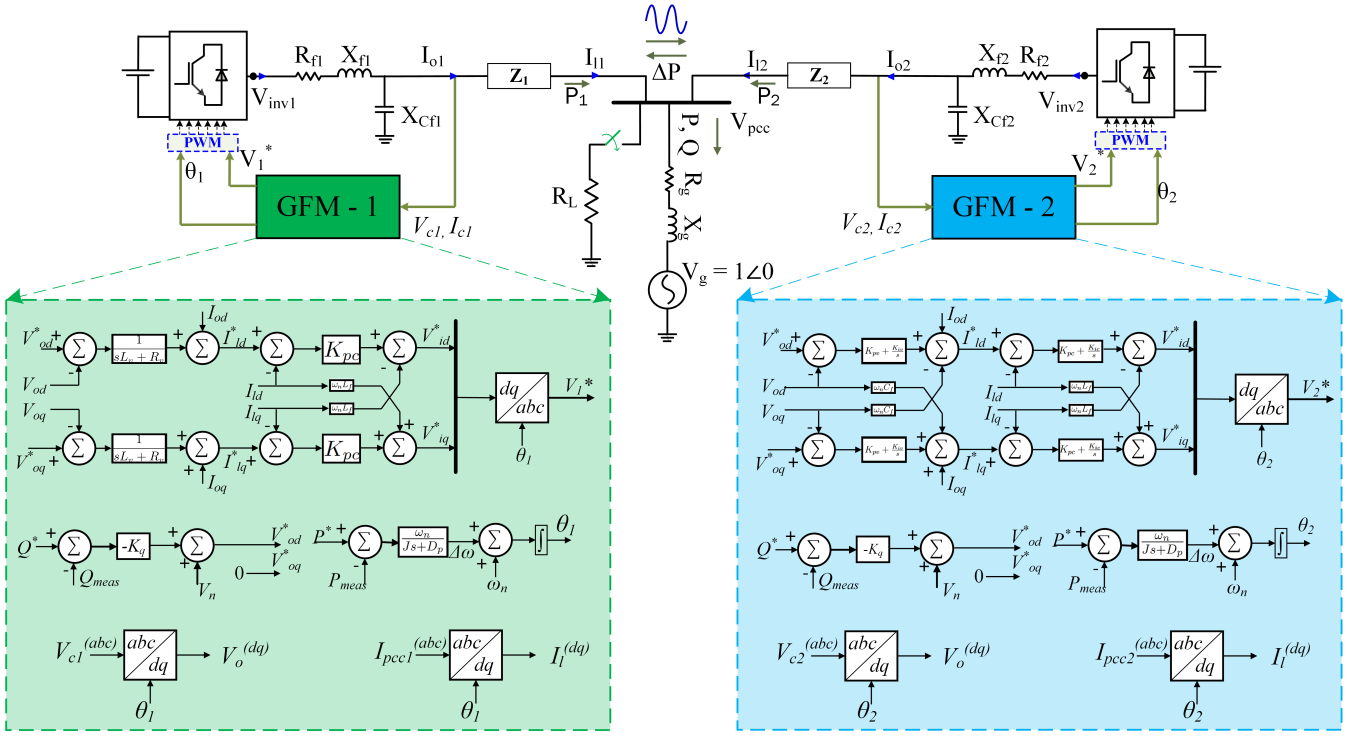

Figure 1. Network layout for GFM interoperability studies. The green box shows the GFM-1 control structure (VAdm control), and the blue box shows the GFM-2 (VSM control). The test network is adapted from (Ghimire et al., 2024) and the GFM control architectures are adapted from (Ghimire et al., 2023).

Here, the simplified representations of two OF-WPPs are connected to the same PCC via individual interconnectors of impedance Z_1 and Z_2, respectively. These respective impedances include the turbine transformer impedance, the array cable impedance, and the park transformer impedance altogether. Further, the power grid is modeled as an ideal voltage source behind a Thevenin equivalent impedance given as $Z_g = R_g + jX_g$.

To study the interoperability of independently designed GFM converters, the generation sources in this test system are equipped with different GFM control methods. GFM-1 is controlled via a virtual admittance (VAdm)-based control method, while GFM-2 is controlled via a virtual synchronous machine (VSM) based control method. The control methods are adapted from (Ghimire et al., 2023), and for a detailed explanation of their control structure and modeling, readers are referred to the same. Notably, these two control methods have identical outer-loop power controller structures and tuning, emulating the synchronous machine's swing equation (Kundur et al., 2017).

https://doi.org/10.5194/wes-2025-18
Preprint. Discussion started: 10 March 2025
© Author(s) 2025. CC BY 4.0 License.

eawe european academy of wind energy
Open Access WIND ENERGY SCIENCE DISCUSSIONS

The mathematical model of the outer power control loop of both VSM and VAdm can be written as:

$$\theta = \int \left[\omega_n + \frac{1}{Js + D_p}(P^* - P_{meas})\right] dt \tag{1}$$

$$V_{od}^* = V_n^* - K_q(Q^* - Q_{meas}), \quad V_{oq}^* = 0 \tag{2}$$

Here, θ is the phase defined by the converter control, $\omega_n := 2\pi f_n$ is the base angular frequency of the power system with the nominal frequency $f_n = 50$ Hz. J and D_p are the virtual inertia constant and damping constant, and P^* and P_{meas} are the active power references and measurements, respectively. Similarly, Q^* and Q_{meas} denote the reactive power references and measurements respectively, V_n^* denotes the voltage reference, and V_{odq}^* denote the direct and quadrature axes voltage references generated by the reactive power control loop.

The inner current and voltage control loops of VSM are PI-controller with dq-axis decoupling and are written as:

$$G_{PI}^v(s) = K_{pv} + \frac{K_{iv}}{s} \tag{3}$$

$$I_{ldq}^* = I_{odq} + G_{PI}^v(s)(V_{odq}^* - V_{odq}) + j\omega_n C_f V_{odq} \tag{4}$$

$$G_{PI}^c(s) = K_{pc} + \frac{K_{ic}}{s} \tag{5}$$

$$V_{idq}^* = V_{gdq} + G_{PI}^c(s)(I_{odq}^* - I_{odq}) + j\omega_n L_f I_{ldq} \tag{6}$$

Here, K_{pv}, K_{iv} and K_{pc}, K_{ic} are the respective PI-gains of the inner loop voltage and current controllers, and V_{odq}, I_{odq} denote the measured voltage and currents while V_{odq}^*, I_{odq}^* denote the reference voltage and currents respectively.

The inner loops for VAdm include a current correction/voltage control via a virtual admittance and a proportional current controller. The control equations are written mathematically as:

$$Y_{virt}(s) = \frac{1}{sL_v + R_v} \tag{7}$$

$$I_{ldq}^* = I_{odq} + (V_{odq}^* - V_{odq})Y_{virt}(s) \tag{8}$$

$$V_{idq}^* = V_{gdq} + K_{pc}(I_{ldq}^* - I_{ldq}) + j\omega_n L_f I_{ldq} \tag{9}$$

Here, L_v, R_v are the virtual inductance and resistance that define the virtual admittance $Y_{virt}(s)$. Also, K_{pc} is the proportional gain for the inner-loop current control.

The current limiting is implemented for the current reference I_{ldq}^* as follows:

$$I_{ldq}^* = \begin{cases} \frac{I_{ldq}^*}{|I_{ldq}^*|}1.2, & \text{if } |I_{dq}| \geq 1.2. \\ I_{ldq}^*, & \text{otherwise.} \end{cases} \tag{10}$$

Here, $|I_{ldq}^*| = \sqrt{(I_{ld}^*)^2 + (I_{lq}^*)^2}$ is the current magnitude.

A simplified electrical representation of the system under study from Fig. 1 is presented in Fig. 2. Here, $Z_{c1,2}$ represent the converter internal impedance with Z_{c1} including the VAdm virtual impedance defined as $Z_{virt} = 1/Y_{virt}$, $Z_{1,2}$ represent the connection impedance, $V_{c1,2}$ represent the converter terminal voltage phasors, $f_{1,2} = \omega_{1,2}/2\pi$ represent the converter-defined

https://doi.org/10.5194/wes-2025-18
Preprint. Discussion started: 10 March 2025
© Author(s) 2025. CC BY 4.0 License.

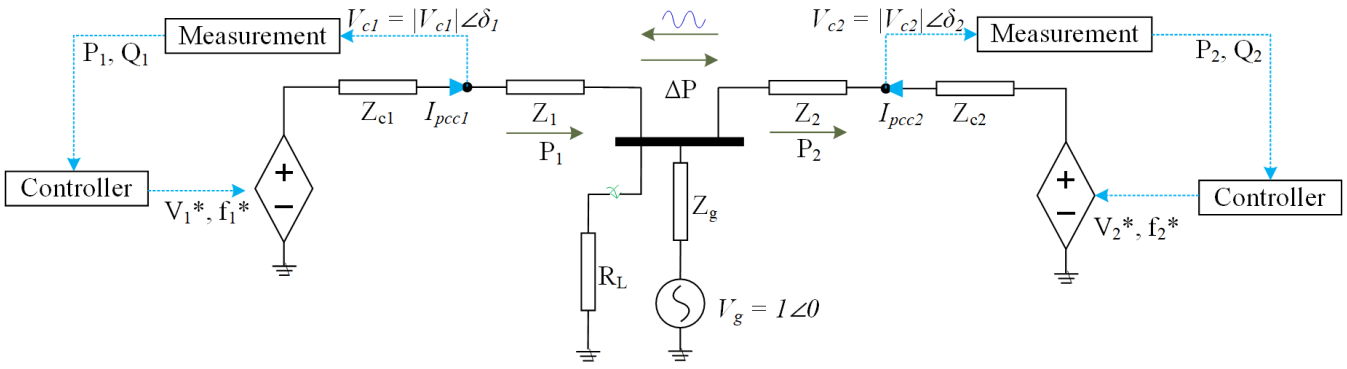

Figure 2. Simplified electrical model of the system under study.

frequency based on their power controller outputs, and ΔP and Δf are the power and frequency oscillations between the converters.

The power and frequency oscillations are given as:

$$\Delta P = \frac{P_1 - P_2}{S_{base}} \tag{11}$$

$$\Delta f = f_1 - f_2 \tag{12}$$

Where S_{base} is the base power for the system. It is recommended that S_{base} be selected to be either as the sum of the converter base powers, i.e., $S_{base} = S_{base1} + S_{base2}$, or as the higher of the two base powers, i.e., $S_{base} = max(S_{base1},\ S_{base2})$. In this paper, since $S_{base1} = S_{base2}$, we have selected $S_{base} = S_{base1}$.

3 Proposed Solution - I: Additional Damping

Since our test case of two GFM converters in nearby WPPs are two voltage sources connected to the same PCC, they attempt to control the voltage at electrically proximal nodes. In this attempt, due to their voltage-source nature, each of the converters opposes the action of the other, thus leading to an oscillatory behavior, as shown in Figure 3. The oscillations here are low frequencies of around $5 - 6\ Hz$. In a GFM converter, the power control loop sets the converter frequency based on the power error (difference between power reference and power demand.) Observing GFM-1 first, the power control loop of the GFM converters adjusts its frequency in an attempt to synchronize with the rest of the system. It changes its power output due to the active power-frequency dependency, which in turn changes the frequency. GFM-2 opposes the frequency change from GFM-1 and adjusts its active power output accordingly. GFM-1 and GFM-2 act in opposition to each other, thus leading to an oscillatory behavior of the active power and frequency. This problem was also identified in the authors' previous paper (Ghimire et al., 2024) and will be solved in this paper.

One way to reduce the oscillations is to regulate the converter-defined frequency so that it attempts to stay at or near a nominal value during the steady state. Here, we propose a frequency regulation via a frequency-active power droop control to create an

https://doi.org/10.5194/wes-2025-18
Preprint. Discussion started: 10 March 2025
© Author(s) 2025. CC BY 4.0 License.

eawe european academy of wind energy
Open Access WIND ENERGY SCIENCE DISCUSSIONS

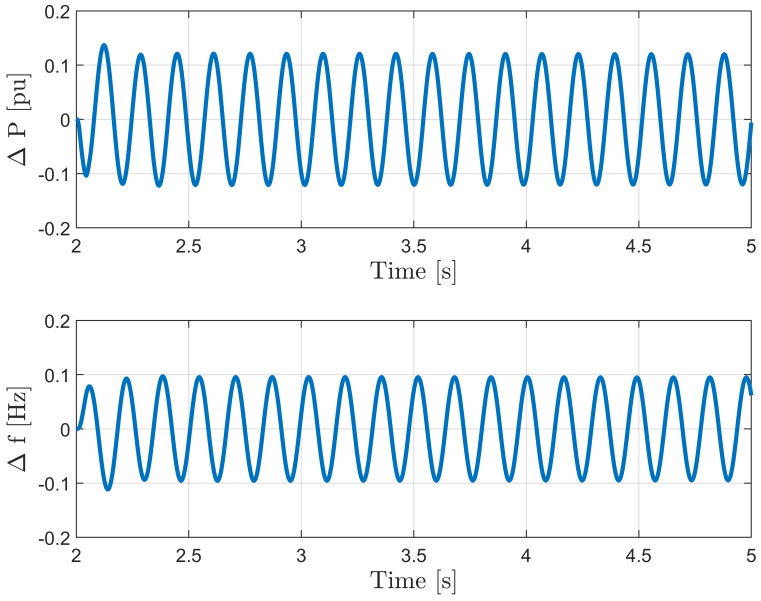

Figure 3. Power and frequency oscillation between GFM-1 and GFM-2 triggered by a phase jump.

active power reference correction $\Delta P_{\omega p}$. This changes the active power reference proportional to the frequency change from the nominal value of ω_n. A low-pass filter (LPF) is added before the droop gain to eliminate any fast transient changes in the frequency since outer control loops, such as the power control loop, should operate slower, and the faster inner control loops will eventually reduce any existing faster transients. The power reference offset defined by the oscillation mitigation strategy is given as follows,

$$\Delta P_{\omega p} = K_{\omega p} \frac{\omega_n}{s + \omega_n} (\omega_n - \omega) \tag{13}$$

where $K_{\omega p}$ is the feedback gain.

Adding the feedback unit opposes the change in system frequency from the nominal of ω_n via a frequency-power droop control. This frequency regulation returns the converter frequency to the nominal stable operating point after a transient, thus stabilizing the system. The LPF ensures the prevention of faster frequency excursions during transient phases. The power reference offset defined by the oscillation mitigation strategy is given as follows,

$$\Delta P_{\omega p} = K_{\omega p} \frac{\omega_n}{s + \omega_n} (\omega_n - \omega) \tag{14}$$

Where ω_n is the filter cut-off frequency and $K_{\omega p}$ is the feedback gain.

The small-signal control diagram of the oscillation mitigation strategy is presented in Fig. 4.

https://doi.org/10.5194/wes-2025-18
Preprint. Discussion started: 10 March 2025
© Author(s) 2025. CC BY 4.0 License.

WIND ENERGY SCIENCE DISCUSSIONS

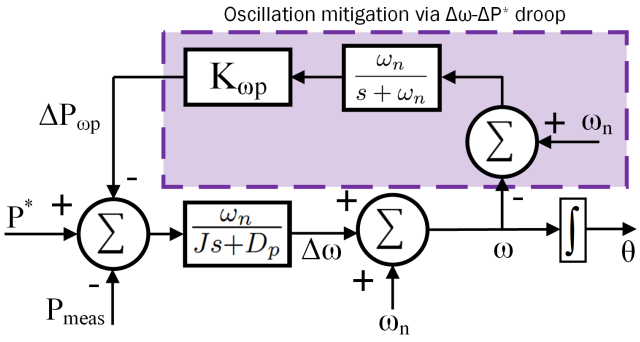

Figure 4. Oscillation mitigation via $\Delta\omega - \Delta P^*$ droop feedback in the power control loop.

Here, the dynamic equation for the power control loop of the GFM converters from eq. (1) changes as follows:

$$\theta = \int \left[\omega_n + \frac{1}{Js + D_p}(P^* - P_{meas} - \Delta P_{\omega p}) \right] dt \tag{15}$$

The overall transfer function from the active power error to the frequency error before the oscillation mitigation strategy is as follows:

$$G_{pc}(s) = \frac{\Delta\omega}{P^* - P_{meas}} = \frac{\omega_n}{Js + D_p}. \tag{16}$$

The transfer function for the oscillation mitigation strategy is written as:

$$G_{\omega p}(s) = \frac{\Delta P_{\omega p}}{\Delta\omega} = K_{\omega p}\frac{\omega_n}{s + \omega_n} \tag{17}$$

Considering the oscillation mitigation strategy, we write for the overall closed-loop transfer function for the power control loop in Fig. 2 as:

$$G_{pcd}(s) = \frac{\Delta\omega}{P^* - P_{meas}} = \frac{G_{pc}(s)}{1 + G_{pc}(s)G_{\omega p}(s)} \tag{18}$$

We can simplify this as:

$$G_{pcd}(s) = \frac{\omega_n(s + \omega_n)}{Js^2 + (J\omega_n + D_p)s + \omega_n(D_p + \omega_n K_{\omega p})} \tag{19}$$

The solution method proposed above is analyzed in the frequency domain in this section to understand the effect of the additional damping on open-loop and closed-loop characteristics of the power controller of the GFM converters.

We use the simple power flow calculation formula to obtain the active power measurement as follows:

$$P_{meas} = \frac{V_b^2}{X_g}\sin(\theta - \theta_g) \tag{20}$$

Here, V_b is the base voltage. The underlying assumption behind this formula is that the grid and converter voltage magnitudes are both at one pu, thus $V_g = V_c = 1\ pu$. Since both the GFM converters and the power grid are ideal voltage sources in the small-signal domain, this assumption is valid for our studies with the small-signal models.

https://doi.org/10.5194/wes-2025-18
Preprint. Discussion started: 10 March 2025
© Author(s) 2025. CC BY 4.0 License.

eawe european academy of wind energy
Open Access WIND ENERGY SCIENCE DISCUSSIONS

In the small-signal domain, we can linearize the sine function as: $\sin(\theta - \theta_g) \approx \cos(\theta_0 - \theta_{g0})(\theta - \theta_g)$. Also, the grid phase θ_g stays constant for small time frames and can be omitted for small-signal studies. Thus, we can write the power measurement for our simplified closed-loop studies as:

$$\Delta P^{pc}_{meas} = \frac{V_b^2}{X_g} \cos\theta_0 \Delta\theta \tag{21}$$

Similarly, for VAdm, due to the effect of the virtual reactor $X_v = \omega_n L_v$, the power calculation changes as follows:

$$\Delta P^{vadm}_{meas} = \frac{V_b^2}{X_g + X_v} \Delta\theta \tag{22}$$

A simplified representation of the small-signal open-loop and closed-loop power controller representation from the power reference P^* input to frequency $\Delta\omega$ is presented in Fig. 5.

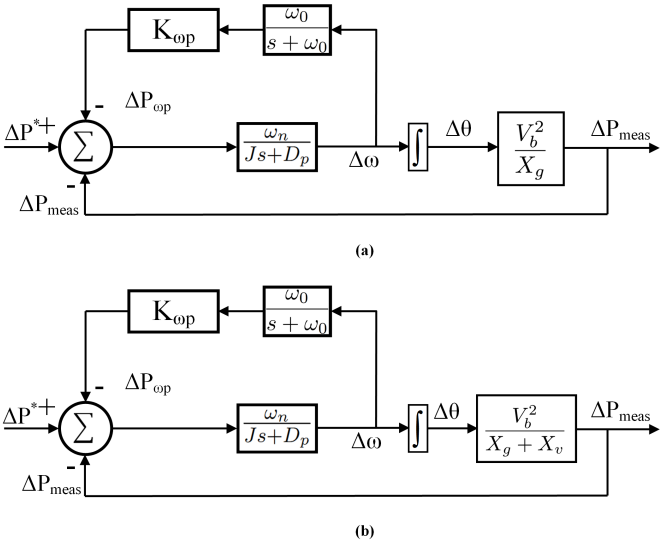

Figure 5. Power controller small-signal model for: (a) VSM, (b) VAdm.

3.1 Open-Loop Analyses

Using the power calculation from equation (21) with the power controller transfer functions in (16) and (19), the open-loop power control transfer functions for VSM can be written as:

$$G^{ol}_{vsm}(s) = G_{pc}(s)\frac{1}{s}\frac{V_b^2}{X_g} \tag{23}$$

$$G^{ol}_{vsmd}(s) = G_{pcd}(s)\frac{1}{s}\frac{V_b^2}{X_g} \tag{24}$$

https://doi.org/10.5194/wes-2025-18
Preprint. Discussion started: 10 March 2025
© Author(s) 2025. CC BY 4.0 License.

eawe european academy of wind energy
Open Access WIND ENERGY SCIENCE DISCUSSIONS

Similarly, for VAdm, we use (22) to write the open-loop transfer function for the power control loop as:

$$G^{ol}_{vadm}(s) = G_{pc}(s)\frac{1}{s}\frac{V_b^2}{X_g + X_v} \tag{25}$$

$$G^{ol}_{vadmd}(s) = G_{pcd}(s)\frac{1}{s}\frac{V_b^2}{X_g + X_v} \tag{26}$$

From this, the open-loop poles of these transfer functions are calculated analytically.

$$\lambda^{ol}_{pc} = 0, -\frac{D_p}{J} \tag{27}$$

$$\lambda^{ol}_{pcd} = 0, -\frac{J\omega_n + D_p}{2J} \pm \frac{1}{2J}\sqrt{(J\omega_n + D_p)^2 - 4J(D_p + \omega_n K_{\omega p})} \tag{28}$$

Here, for our parameter selection, the open-loop poles of both the power controller transfer functions lie on the left half of the s-plane, and thus both the power controller realizations are open-loop stable. Further, it is notable that these open-loop eigenvalues are independent of the grid SCR, and no SCR sweep is necessary to understand their loci further.

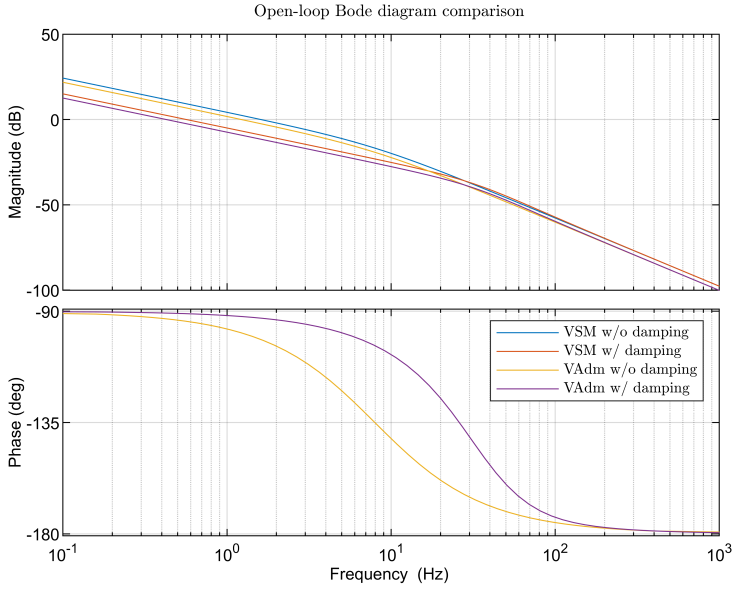

Figure 6. Open loop bode diagram of the power controller with and without the $K_{\omega p}$ damping.

The respective bode diagrams of the open-loop controls are given in Fig. 6. The bode diagrams here show that the open-loop phase margin of the power controller is improved with the addition of the damping term. Table 1 summarizes the system stability metrics.

Although the control changes have led to an increase in open loop bandwidth and a reduction in DC gain, the phase margin has only changed slightly, keeping the overall stability intact.

https://doi.org/10.5194/wes-2025-18
Preprint. Discussion started: 10 March 2025
© Author(s) 2025. CC BY 4.0 License.

eawe european academy of wind energy
Open Access WIND ENERGY SCIENCE DISCUSSIONS

Table 1. Open loop stability metrics for the power controller.

Metric	Without Damping	With Damping
Phase Margin	99.16° at 310.15 rad/s	104.40° at 334.22 rad/s
Gain Margin	∞	∞
Bandwidth	49.88 rad/s	141.49 rad/s
DC Gain	15.95 dB	9.09 dB

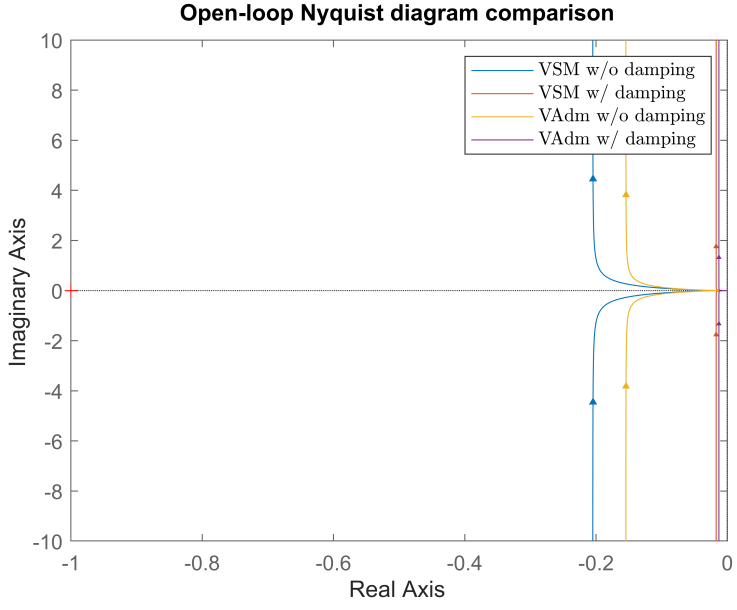

Figure 7. Open-loop Nyquist plot of the power control with and without the additional $K_{\omega p}$ damping term.

Further, in Fig. 7, the Nyquist plots of the open-loop system show that system stability is not compromised by the addition of the feed-back damping term in the power controller as a solution method for interoperability issues.

Further information on system stability is extracted from closed-loop analysis.

3.2 Closed-Loop Analyses

Although open-loop analysis provided us with some crucial information on system small-signal stability, a closed-loop analysis is necessary for the complete picture of system stability. The respective closed-loop transfer functions for both the cases with

https://doi.org/10.5194/wes-2025-18
Preprint. Discussion started: 10 March 2025
© Author(s) 2025. CC BY 4.0 License.

eawe european academy of wind energy
Open Access WIND ENERGY SCIENCE DISCUSSIONS

and without the damping terms are given as:

$$G^{cl}_{vsm}(s) = \frac{G^{ol}_{vsm}(s)}{1+G^{ol}_{vsm}(s)} \tag{29}$$

$$G^{cl}_{vsmd}(s) = \frac{G^{ol}_{vsmd}(s)}{1+G^{ol}_{vsmd}(s)} \tag{30}$$

$$G^{cl}_{vadm}(s) = \frac{G^{ol}_{vadm}(s)}{1+G^{ol}_{vadm}(s)} \tag{31}$$

$$G^{cl}_{vadmd}(s) = \frac{G^{ol}_{vadmd}(s)}{1+G^{ol}_{vadmd}(s)} \tag{32}$$

$$\tag{33}$$

Here, the equations respectively denote the closed-loop transfer function of VSM without the $K_{\omega p}$ damping, VSM with the $K_{\omega p}$ damping, VAdm without the $K_{\omega p}$ damping, and VAdm with the $K_{\omega p}$ damping.

An SCR sweep from 1 to 10 with an increment of 0.1 is performed to understand the eigenvalue characteristics of the closed-loop power controller transfer function. It is presented in Fig. 8.

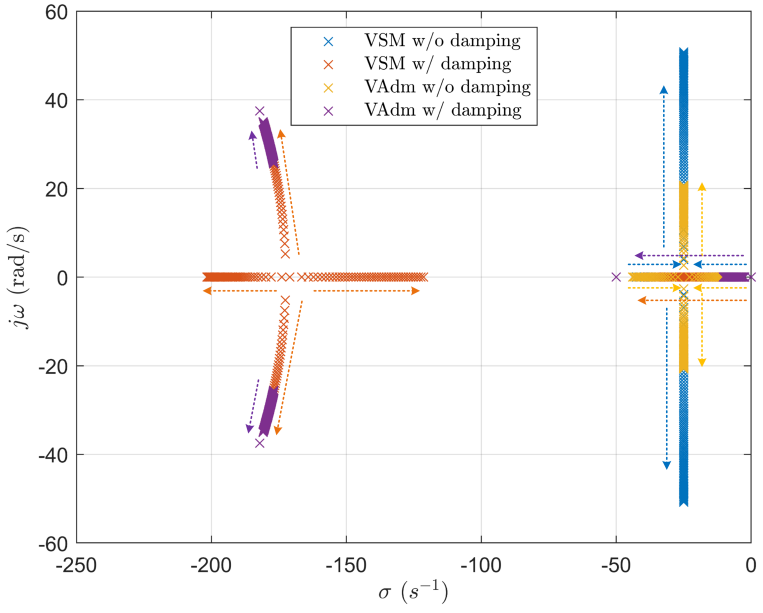

Figure 8. Close loop eigenvalue plots of the power controller with an SCR sweep from 1 to 10. The arrowheads represent higher SCR values.

The closed-loop system eigenvalues show that some eigenvalues' damping ratios decrease with the increase in grid strength. However, their overall stability is improved by adding the $K_{\omega p}$ damping term in the power control loop. Even for such a wide range of system SCR values, the system maintains small-signal stability, and the dominant poles move toward the left side of the s-plane.

https://doi.org/10.5194/wes-2025-18
Preprint. Discussion started: 10 March 2025
© Author(s) 2025. CC BY 4.0 License.

eawe european academy of wind energy
Open Access WIND ENERGY SCIENCE DISCUSSIONS

Fig. 9 shows the respective bode diagrams of the closed-loop controls. The bode diagrams show that the control change does not severely affect the control performance. Although some differences could be observed around the corner frequency.

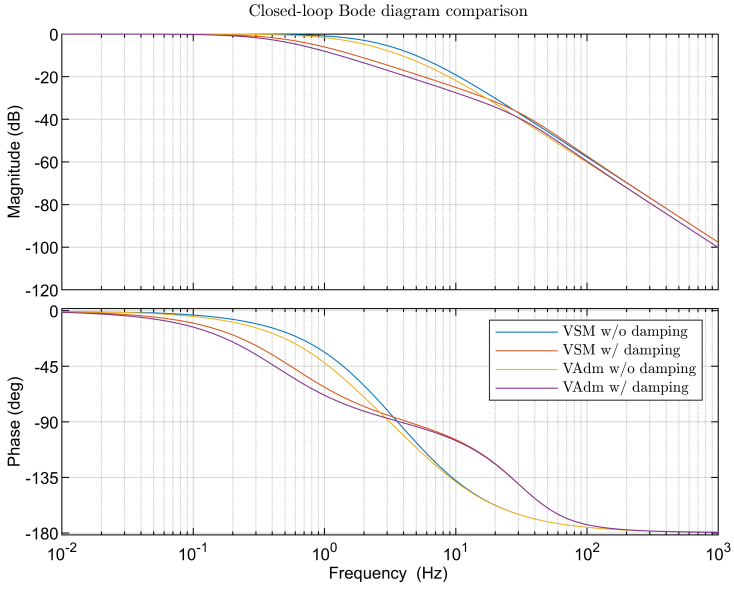

Figure 9. Close loop bode diagram of the power controller with and without the $K_{\omega p}$ damping.

Figure 10 shows the step response of the closed-loop power controllers. This indicates that the $K_{\omega p}$ damping term slows the power controller response and increases the overall damping.

Further, impulse responses in Figure 11 show that the $K_{\omega p}$ damping term reduces the peak of the impulse response and improves the overshoot in the system.

A summary of the power controller open loop and closed loop responses are presented in Table 2.

Table 2. Open-loop and closed-loop performance of power control loops.

Control Mode	T_{rise}	$T_{settling}$	Bandwidth	Phase Margin
VSM w/o $K_{\omega p}$	0.1716	0.3077	2.01 Hz	78.6°
VSM w $K_{\omega p}$	0.6108	1.0924	0.57 Hz	89°
VAdm w/o $K_{\omega p}$	0.2408	0.4376	1.44 Hz	81.9°
VAdm w $K_{\omega p}$	0.8137	1.4536	0.43 Hz	89.3°

Closed-loop analysis showed that the $K_{\omega p}$ damping term increases the power controller's rise time and settling time. Further, it reduces the power controller bandwidth, while the open-loop phase margin is improved with the damping term.

https://doi.org/10.5194/wes-2025-18
Preprint. Discussion started: 10 March 2025
© Author(s) 2025. CC BY 4.0 License.

eawe european academy of wind energy
Open Access WIND ENERGY SCIENCE DISCUSSIONS

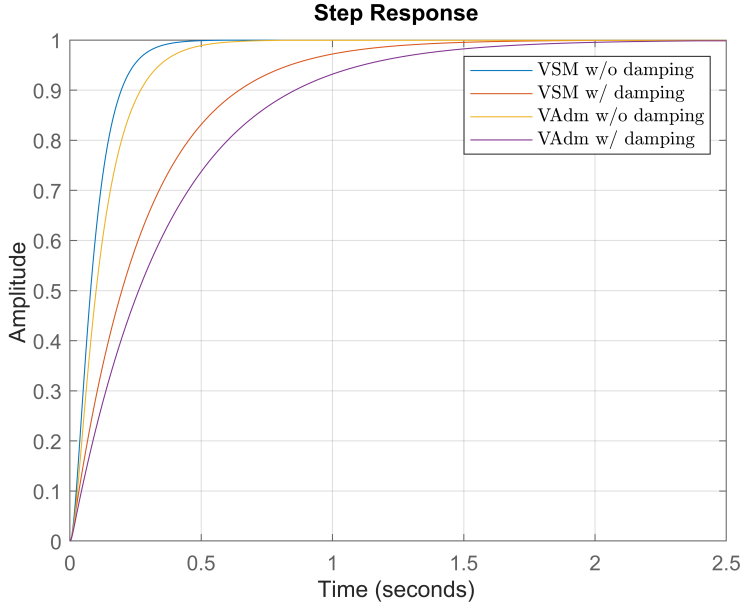

Figure 10. Step responses of the closed-loop power controller.

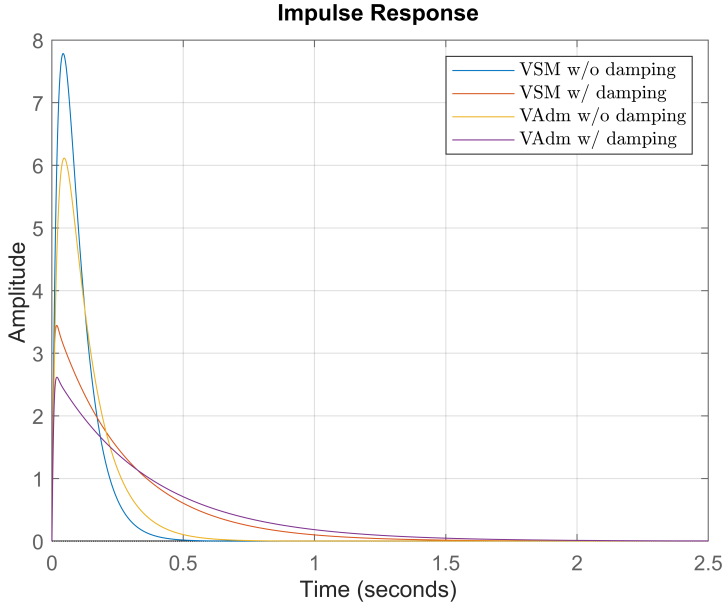

Figure 11. Impulse responses of the closed-loop power controller.

https://doi.org/10.5194/wes-2025-18
Preprint. Discussion started: 10 March 2025
© Author(s) 2025. CC BY 4.0 License.

eawe european academy of wind energy
Open Access WIND ENERGY SCIENCE DISCUSSIONS

4 Response to System and Grid Events

Although the small-signal studies presented in section 3 provide a good insight into small-signal frequency-domain behavior and stability, time-domain simulation and studies are crucial for understanding the dynamic operation and stability of our multi-converter system. A study of the GFM converters' responses to different grid events is crucial and was performed in the previous paper as well (Ghimire et al., 2024). Here, we continue the studies with various simulated grid events to study potential system oscillations. The results are presented herewith.

4.1 Load Addition

Firstly, in response to a load addition of 0.05 pu at the PCC, the converters react to it by providing an active power response that lasts for a transient period before settling to the pre-event steady-state value. The power and frequency of each GFM converter and their interactions are shown in Fig. 12.

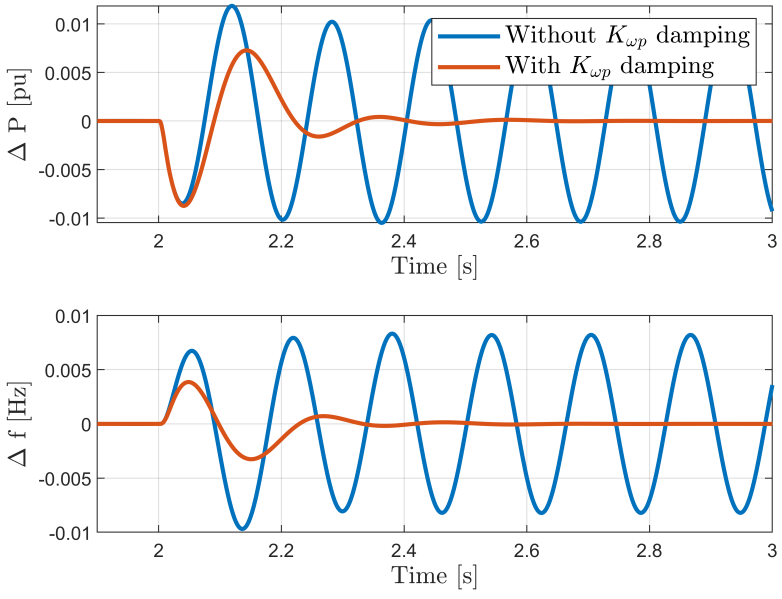

Figure 12. Converters responses to load addition of 0.05 pu.

Here, it is clearly seen that the converters exhibit a low-amplitude oscillation of around 5 Hz in power and frequency, which damps out within 400 ms, showing that the oscillation mitigation strategy proposed in Section 3 improves the dynamic performance during load-addition event by providing improved damping to the power controller.

https://doi.org/10.5194/wes-2025-18
Preprint. Discussion started: 10 March 2025
© Author(s) 2025. CC BY 4.0 License.

eawe european academy of wind energy
Open Access WIND ENERGY SCIENCE DISCUSSIONS

4.2 Phase Shift

Further, a grid phase shift of 4.5° is applied to the system, and the converter responses are recorded. Here, both converters react to the system event with a synchronizing active power response, which leads to a damped oscillation of around 5 Hz with a settling time of 400 ms, as shown in Fig. 13. This is a well-damped oscillation in a system of multiple voltage source converters connected to an electrically proximal point. This illustrates the applicability of our proposed method for oscillation mitigation in another grid event.

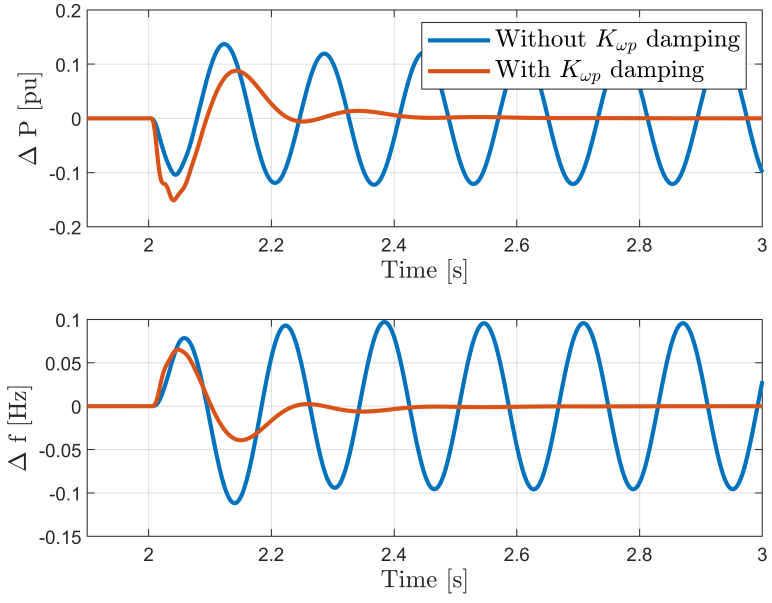

Figure 13. Converters responses to a phase shift of 4.5°.

4.3 Grid Voltage Sag

Similarly, in response to a grid voltage drop of 5% from nominal, Fig. 14 shows that the GFM converters exhibit similar responses as in the previous two cases – a well-damped transient active power and frequency oscillation of around 5 Hz with a settling time of 500 ms – demonstrating the applicability of the oscillation mitigation method proposed in Section 3.

4.4 Grid RoCoF

Finally, we test our mitigation method against another important grid event–RoCoF. A grid RoCoF of -0.5 Hz/s is applied to the ideal voltage source behind the grid Thevenin impedance for 400 ms. After 200 ms, the RoCoF event ends, and the grid frequency attains a new state of 49.9 Hz.

https://doi.org/10.5194/wes-2025-18
Preprint. Discussion started: 10 March 2025
© Author(s) 2025. CC BY 4.0 License.

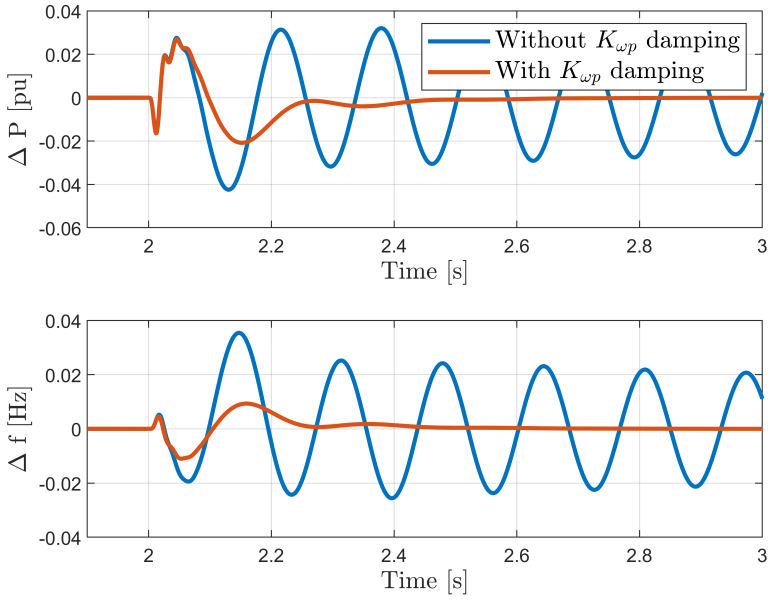

Figure 14. Converters responses to a voltage drop of 5% from nominal.

The converters' response to the RoCoF event is presented in Fig. 15. When the converters respond to the RoCoF event, their responses are normal and within the bounds of the acceptable system power and frequency limits. However, as soon as the grid frequency attains a newer state than the nominal frequency, the converters' responses start to diverge: frequencies start to swell, and the active power starts to drop, leading to complete instability.

This shows that the proposed oscillation mitigation strategy does not apply to a grid RoCoF event. However, to solve this issue of the inability of the GFM converters to ride through a grid-RoCoF event, understanding the responses and the underlying reason is crucial.

A zoomed-in view of the converter responses during and immediately after the RoCoF event is presented in Fig. 16. The converters respond inherently to the RoCoF without any signs of instability; however, as the RoCoF event finishes and the grid frequency settles at the new frequency level of 49.9 Hz, the converter response starts to diverge from its steady state, and instability is observed.

From these results, it could be inferred that although this method successfully eliminates the inter-converter operation and boosts interoperability, since it tries to regulate the frequency at the nominal ω_n, the system stability is compromised for a grid RoCoF, especially if the grid frequency settles at a different level than ω_n. During a grid RoCoF, the GFM converter attempts to supply an inertial active power response and change its frequency to do so. However, the $\Delta\omega - \Delta P^*$ droop feedback attempts to control the system frequency at the rated ω_n, thus leading to oscillatory instability.

https://doi.org/10.5194/wes-2025-18
Preprint. Discussion started: 10 March 2025
© Author(s) 2025. CC BY 4.0 License.

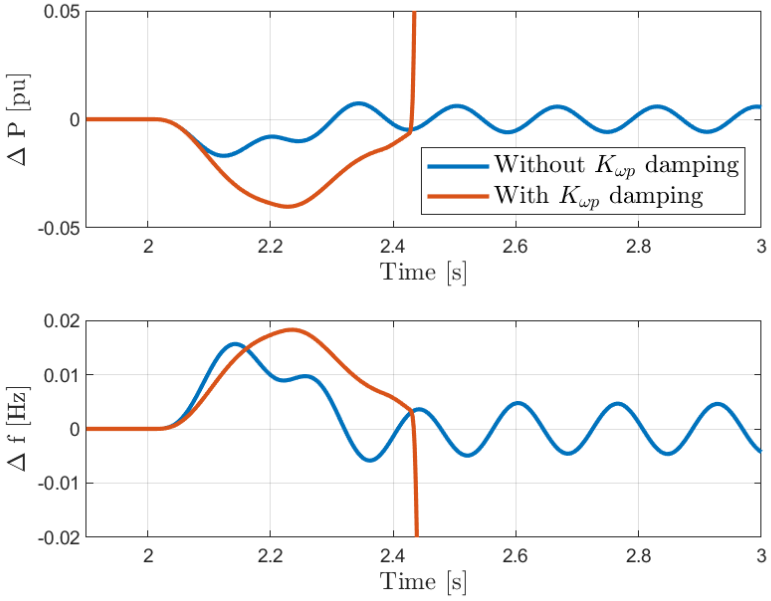

Figure 15. Converters responses to a RoCoF of -0.5 Hz/s from nominal.

An adaptation to the solution method proposed in Section 3 is required to adapt the GFM power controllers' frequency output based on steady-state grid frequencies while still staying inert to fast grid frequency excursions. Thus, an adapted method to enable the operation of the GFM converters with an enhanced $\Delta\omega - \Delta P$ damping with the possibility of the GFM converters staying stable at steady grid frequencies away from the nominal value is presented in the following section.

5 Proposed Solution - II: PLL-Reinforced Damping

The oscillation mitigation method proposed in Fig. 4 provides an additional damping via $\Delta\omega - \Delta P^*$ droop. However, as seen in Section 4, any steady-state change in grid frequency leads to instability. As explained earlier in the paper, the reason for the instability is the converter's inability to maintain the frequency at/around the set-point defined by ω_n in the solution method proposed in Fig. 4. In this section, we propose an improvement in the method to enable operation during steady-state changes in grid frequency.

Instead of providing a droop-response to the power reference based on the converter-defined frequency and a frequency set-point ω_n as shown in Fig 4, we can reinforce the damping provided by the $\Delta\omega - \Delta P^*$ droop feedback loop via a PLL. A schematic diagram illustrating this method is presented in Fig. 17 below.

This PLL-based damping with a filter ensures that the converters track the long-term steady-state grid frequency changes while staying inert to transient and fast grid frequency excursions. In cases where the power grid settles at a new frequency

https://doi.org/10.5194/wes-2025-18
Preprint. Discussion started: 10 March 2025
© Author(s) 2025. CC BY 4.0 License.

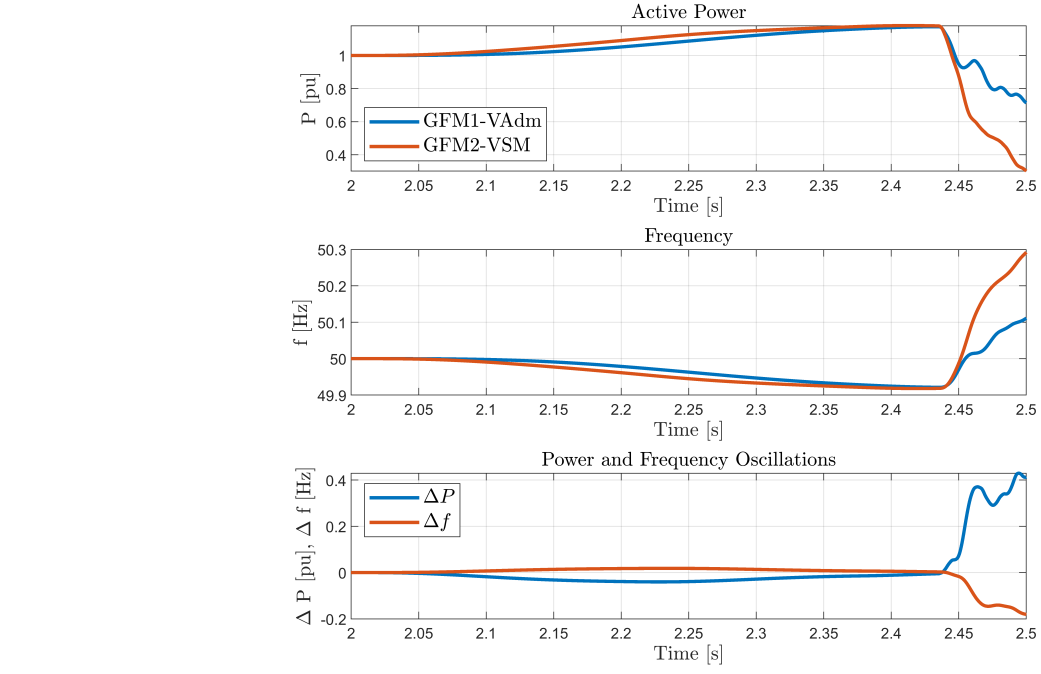

Figure 16. RoCoF response (zoomed in) of the system with the $K_{\omega p}$ damping based oscillation mitigation strategy. Nominal case without the $K_{\omega p}$ damping is not presented.

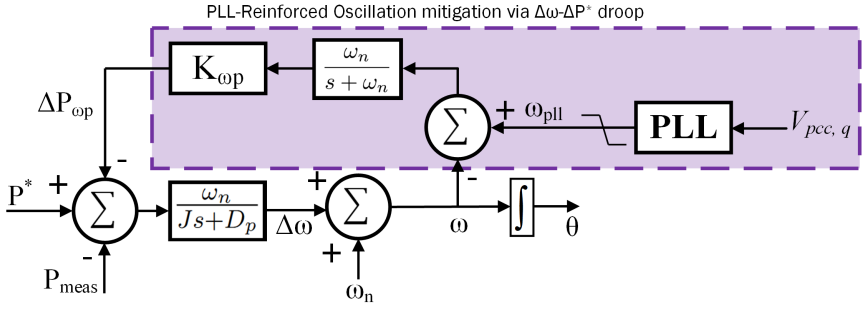

Figure 17. Oscillation mitigation via $\Delta\omega - \Delta P^*$ droop feedback in the power control loop with frequency setpoint provided by a PLL.

https://doi.org/10.5194/wes-2025-18
Preprint. Discussion started: 10 March 2025
© Author(s) 2025. CC BY 4.0 License.

eawe european academy of wind energy
Open Access WIND ENERGY SCIENCE DISCUSSIONS

$\omega \neq \omega_n$, the GFM converters will not attempt to stay at the nominal frequency (ω_n), leading to system instability; however, they will attempt to track the grid frequency and ensure system stability.

A similar approach is proposed in the patent (Schweizer et al., 2021); however, the patent is not focused on oscillation mitigation. The patent relates to fault ride-through and switching between PLL-based and VSM P-loop-based synchronizations during different operation phases. Further, an impedance-based analysis of a similar control realization could be seen in (Shah et al., 2024); thus, this paper does not present impedance-based analysis/studies of the proposed oscillation mitigation method. This method is also similar to the mechanical governor action in a synchronous machine given by a large time constant of the governor. However, our approach is neither employed for switched operations between PLL and VSM P-loop during different operating conditions nor for general steady-state stability. Our approach reinforces the power controller during its operation with the aid of a PLL and enhances the interoperability of a multi-converter system.

Now, applying this solution method to the power control loops and applying the same grid RoCoF event to our test system, Fig. 18 shows that the converters' responses to the event are now stable both during the event and after the grid attains a new steady state in its frequency.

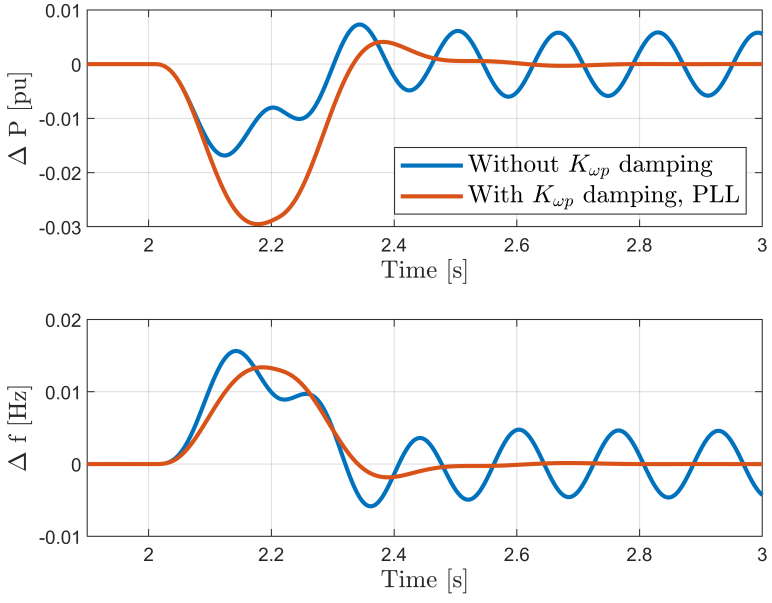

Figure 18. RoCoF response of the GFM converters before and after the inclusion of PLL-reinforcement method for oscillation mitigation via $\Delta\omega - \Delta P^*$ droop feedback in the power control loop.

Here, the converters now – contrary to the instability seen in Fig. 15 and in Fig. 16 – react to the RoCoF event with an active power response during the event duration and following the event attain a new active power operating point corresponding to the new frequency state of the grid.

https://doi.org/10.5194/wes-2025-18
Preprint. Discussion started: 10 March 2025
© Author(s) 2025. CC BY 4.0 License.

eawe european academy of wind energy
Open Access WIND ENERGY SCIENCE DISCUSSIONS

6 Conclusions

The studies presented in this paper showed that the interoperability of independently designed GFM converters connected with high electrical proximity in a multi-converter system can lead to control oscillations that can adversely affect the system's stability. The solution methods proposed in this paper reinforced the power control loop with a fixed frequency setpoint or a PLL-derived frequency setpoint. This successfully improved the dynamic performance of the independently designed GFM converters in the multi-converter system. They improved interoperability with a small cost of closed-loop small-signal performance. The power controller damping was improved without severely slowing its overall response. The power and frequency oscillations were successfully reduced during several crucial grid events.

Since the control changes suggested in this paper are on the power control/synchronization loop, which is present in all GFM converters, one can apply the oscillation mitigation strategy suggested by our paper on other power synchronization loops, such as PI-based or droop-based controls. In an extension, with suggestions from TSOs and developers, OEMs can independently make such control updates in their GFM converters' outer power control loop when their GFM converters are expected to connect to other GFM converters in close electrical proximity where understanding the full control model of the other device is impossible for control re-tuning to improve interoperability. Thus, the method presented in our paper can be crucial in improving the stability and interoperability of multi-vendor systems or power systems with multiple GFM converters from different vendors connected to electrically proximal points.

The solution method provided in this paper is helpful for power systems where multiple independently designed GFM converters are connected in close electrical proximity. The proposed method does not require knowledge of the control architecture and tuning of the individual converters connected to the system. It can generally be applied to all power controller setups used in GFM converters for synchronization and outer-loop control.

Future works could consider the impact of PLL dynamics on the closed-loop performance of the solution method proposed. Furthermore, the study of individual converter impedance and its effect on oscillation could be a potential research topic.

Appendix A: Simulation Parameters

The control and electrical parameters used in this paper are summarized in Table A1 below.

Author contributions. SG wrote the original draft. GA and KVK supported the small-signal analysis and time-domain simulations and helped formulate paper contents. KHJ provided guidelines and prepared the plans for the research as part of the funding application. KHJ and GY contributed to the guidance, revisions, and corrections.

Competing interests. The authors declare no competing interests.

https://doi.org/10.5194/wes-2025-18
Preprint. Discussion started: 10 March 2025
© Author(s) 2025. CC BY 4.0 License.

eawe european academy of wind energy
Open Access WIND ENERGY SCIENCE DISCUSSIONS

Table A1. System parameters used in the simulation studies. All parameters are in pu unless otherwise stated.

Parameter	Notation	Value
Filter inductance	X_f	0.0265
Filter resistance	R_f	0.0063
Filter capacitance	C_f	5×10^{-6}
Virtual inertia	J	1 s
Damping constant	D_p	50
Filter cut-off frequency	ω_n	$2\pi 50$ rad/s
Reactive power droop	K_q	0.2
Voltage controller P-gain	$K_p^{(vc)}$	0.05
Voltage controller I-gain	$K_i^{(vc)}$	0.039
Current controller P-gain	$K_p^{(cc)}$	10.5
Current controller I-gain	$K_i^{(cc)}$	16
Virtual impedance	$R_v + j\omega_n L_v$	0.01 + j0.2
$\Delta\omega - \Delta P$ feedback gain	$K_{\omega p}$	$1.8D_p$
Wind turbine base power	S_{base}	8 MVA
Wind turbine base voltage	V_{base}	690 V
PLL PI gains	K_p^{pll}, K_i^{pll}	0.025, 1.5
PLL Bandwidth	$\Delta\omega_{PLL}$	7.5 Hz

Disclaimer. Figures and values presented in this paper should not be used to judge the performance of Siemens Gamesa (SGRE) technology as they are solely presented for demonstration purposes. Any opinions or analyses contained in this paper are the opinions of the authors and are not necessarily the same as those of SGRE.

Acknowledgements. The work of S.G. was supported by Innovation Fund Denmark under the project Ref. no. 0153-00256B. The authors would like to acknowledge the support of Siemens Gamesa Renewable Energy (SGRE), Technical University of Denmark (DTU), and Innovation Fund Denmark. The authors thank Paul Brogan from SGRE, Glasgow, UK, and Thyge Knueppel from SGRE, Copenhagen, Denmark, for their guidance, help, and support during the studies performed in this paper.

https://doi.org/10.5194/wes-2025-18
Preprint. Discussion started: 10 March 2025
© Author(s) 2025. CC BY 4.0 License.

eawe european academy of wind energy
Open Access WIND ENERGY SCIENCE DISCUSSIONS

References

Benedetti, L., Papadopoulos, P. N., and Egea-Álvarez, A.: Small Signal Study of Grid-forming Converters and Impact of Different Control Structures and Parameters, in: 2022 IEEE PES Innovative Smart Grid Technologies Conference Europe (ISGT-Europe), pp. 1–5, https://doi.org/10.1109/ISGT-Europe54678.2022.9960644, 2022.

Denninger, R., Erckrath, T., Ernst, P., Rogalla, S., Singer, R., Unruh, P., Jung, M., and Brandl, R.: Case Study: Interoperability of Two Independently Designed Grid-Forming Converters, in: 23rd Wind & Solar Integration Workshop, Helsinki, Finland, 8–11 October 2024, 2024.

Ghimire, S., Kkuni, K. V., Jakobsen, S. C., Knueppel, T., Jensen, K. H., Guest, E., Rasmussen, T. W., and Yang, G.: Grid-forming control methods for weakly connected offshore WPPs, in: 22nd Wind and Solar Integration Workshop (WIW 2023), vol. 2023, pp. 246–253, https://doi.org/10.1049/icp.2023.2744, 2023.

Ghimire, S., Kkuni, K. V., Guerreiro, G. M. G., Guest, E. D., Jensen, K. H., and Yang, G.: Oscillations between Grid-Forming Converters in Weakly Connected Offshore WPPs, in: 2024 IEEE Power & Energy Society General Meeting (PESGM), pp. 1–5, https://doi.org/10.1109/PESGM51994.2024.10689212, 2024.

IEEE Std 1204-1997: IEEE Guide for Planning DC Links Terminating at AC Locations Having Low Short-Circuit Capacities, IEEE Std 1204-1997, pp. 1–216, https://doi.org/10.1109/IEEESTD.1997.85949, 1997.

InterOPERA Consortium: Multi-Party Cooperation Framework, Tech. Rep. D4.2, InterOPERA Project, https://interopera.eu/wp-content/uploads/files/deliverables/InterOPERA-D4.2-Multi-Party-Cooperation_Framework-202312.pdf, accessed: 2024-12-13, 2023.

Kundur, P. S., Balu, N. J., and Lauby, M. G.: Power system dynamics and stability, Power system stability and control, 3, 700–701, 2017.

Maleki, S., Chakraborty, T., Yancey, B., Chen, A. K., and Trahan, H.: Utility-Based Grid Forming Inverters Applications: Seamless Transition and Power Oscillation Damping, in: 2022 IEEE/PES Transmission and Distribution Conference and Exposition (T&D), pp. 1–5, https://doi.org/10.1109/TD43745.2022.9816961, 2022.

Piepka, L., Schöll, C., and Gerber, L.: Power Oscillation Damping with Grid-Forming Converters: A Simulative and System-Theoretical Analysis, in: 23rd Wind & Solar Integration Workshop, Helsinki, Finland, 8–11 October 2024, 2024.

Schweizer, M., Almer, S., and Harnefors, L.: Grid-forming vector current control, https://worldwide.espacenet.com/patent/search/family/068762667/publication/EP3832829A1, 2021.

Shah, C. R., Molinas, M., Nilsen, R., and Amin, M.: Impedance Reshaping of GFM Converters with Selective Resistive Behaviour for Small-signal Stability Enhancement, in: 2024 IEEE Applied Power Electronics Conference and Exposition (APEC), pp. 1619–1626, https://doi.org/10.1109/APEC48139.2024.10509416, 2024.

Tayyebi, A., Groß, D., Anta, A., Kupzog, F., and Dörfler, F.: Interactions of grid-forming power converters and synchronous machines, arXiv preprint arXiv:1902.10750, https://arxiv.org/abs/1902.10750, 2019.

Working Group on Wind Farm Connection: Connection of Wind Farms to Weak AC Networks, Technical brochures, CIGRE Study Committee WG B4.62, https://e-cigre.org/publication/671-connection-of-wind-farms-to-weak-ac-networks, 2016.